Multifractal Analysis of Choroidal SDOCT Images in the Detection of Retinitis Pigmentosa

Francesca Minicucci , Fotios D. Oikonomou , Angela A. De Sanctis *

Posted Date: 16 February 2024

doi: 10.20944/preprints202402.0883.v1

Keywords: Retinitis pigmentosa; choroid; spectral domain optical coherence tomography; multifractal analysis; generalized Renyi point-centered dimensions

 doi:10.20944/preprints202402.0883.v1

Article

Multifractal Analysis of Choroidal SDOCT Images in the Detection of Retinitis Pigmentosa

Francesca Minicucci [1], Fotios D. Oikonomou [2] and Angela A. De Sanctis [3,*]

[1] University of L'Aquila (IT); francesca.minicucci@gmail.com
[2] University of Patras (GR); pheconom@upatras.gr
[3] University «G. d'Annunzio» of Chieti-Pescara (IT); a.desanctis@unich.it
* Correspondence: a.desanctis@unich.it

Abstract: The aim of this paper is to investigate whether multifractal analysis can be applied to study choroidal blood vessels and help ophthalmologists for the early diagnosis of retinitis pigmentosa (RP). In a case study, we use Spectral Domain Optical Coherence Tomography (SDOCT), which is a non-invasive and highly sensitive imaging technique of the retina and choroid. The image of a choroidal branching pattern can be regarded as a multifractal. Therefore, we calculate generalized Renyi point-centered dimensions, which is considered a measure of inhomogeneity of data, to prove that it increases in the patients with RP with respect to the control group.

Keywords: retinitis pigmentosa; choroid; spectral domain optical coherence tomography; multifractal analysis; generalized Renyi point-centered dimensions

1. Introduction

Retinitis pigmentosa is a rare hereditary degenerative pathology of the chorio-retina, characterized by the presence of pigment in the retina. Its clinical presentation can be extremely variable from patient to patient, though maintains some common characteristics, [1,2]. It is caused by a mutation of a gene involved in the molecular cycle of vision, performed by retinal photoreceptors, [3].

The clinical diagnosis of retinitis pigmentosa is based on:

- Night – blindness (nyctalopia), that is, difficulties in night vision
- Reduced visual acuity
- A typical hyperpigmentation of the retina in a "bone spicule" pattern in the mid-periphery, visible by fundoscopy
- Attenuation of retinal arteries
- Dysfunction of photoreceptors, distinguishable by electroretinographical abnormalities
- A peripheral ring scotoma and narrowing of the visual field (detectable by visual field testing)

Histologically RP is identified by rod photoreceptor death followed by cone photoreceptor death at the more advanced stages of disease, resulting in thinning of the outer retinal layers and retinal vessels, waxy pallor of the optic nerve, and pigmentary changes of the retina.

Several genes, if mutated, can lead to RP, but a mutation in whatever of those genes is enough to cause the illness, and this also explains why this pathology is so heterogeneous. RP is usually classified into three subtypes according to the inheritance model: autosomal dominant, autosomal recessive, or X-linked.

The total of clinical variants, syndromic and non- syndromic, has a variable prevalence in different populations which were studied. The global worldwide is 1 case each 3,000-5,000 inhabitants (about 1.5 million cases in the world).

The early diagnosis of RP represents the actual and only defense against this illness. Due to, till nowadays, neither complete healing nor sight recovery, the only possibility for a cure is to slow down the illness progression through daily assumption of vitamin A, omega-3 and lutein. The most recent and advanced kind of treatment is the gene therapy, achieved using stem cells.

 doi:10.20944/preprints202402.0883.v1

We recall that the eye is composed of three overlapping layers, from the innermost to the outermost: retina, uvea and sclera. The retina is the innermost layer of the eyeball and is constituted by neurons. It is sensitive to light stimuli and here starts the visual process. The choroid is part of the uvea, its nature is essentially vascular, and its task is to supply the retina, on the inner side, and sclera, on the outer side, [4].

The retina is of fundamental importance to ophthalmologists because it is where the visual process begins, therefore the retinal diseases are the main cause of blindness in the world.

The retina appears as sophisticated *network of blood vessels.* The development of such a network tends to seek configurations that minimize operational energy expenditure to deliver nutrients and carries aways waste. Often vascular diseases can manifest as abnormalities in this network and thus retinal vascularization offers a way to acquire insight into the presence (or absence) of disease.

From the geometrical point of view, the typical branching shape of retinal blood vessels is a *fractal*, [5], which means an object that reproduces the same pattern on different levels of scale. The fractal dimension FD, [6], provides a measure of the fractal's global complexity. It is well known that for such kind of objects the dimension is not an integer number. Due to the retinal blood vessels grow through the diffusion of angiogenic factors in the retinal plane, the fractal dimension lies between 1 and 2: that means its branching pattern fills space more than a line, but less than a plane. In healthy human subjects, the retinal FD has been proved is around 1.7, but can be altered by the rarefaction or proliferation of blood vessels in the disease scenario. In [7], the authors summarize the current scientific literature on the association between FD and retinal disease.

The main imaging techniques to study the chorio-retina and therefore used in RP diagnosis, [8], are:

- **fundus image photography**
- **Optical Coherence Tomography (OCT)**

The first technique is the traditional way to identify abnormalities in the eye fundus.

Optical coherence tomography (OCT) is a new noninvasive diagnostic imaging modality enabling *in vivo* three-dimensional (3D) visualization of tissue microstructure. Novel high-speed detection techniques and light source technology have revolutionized imaging performance and clinical feasibility of OCT paving the way for cellular resolution retinal imaging and wide-field 3D choroidal visualization for routine clinical diagnosis.

Furthermore, extensions of OCT have been developed that enable noninvasive depth-resolved functional imaging of the retina, providing spectroscopic, blood flow, or physiologic tissue information. These extensions should not only improve image contrast but should also enable the differentiation of retinal pathologies through localized functional states.

Among these, **Optical Coherence Tomography Angiography (OCTA)** allows indirect visualization of the chorio-retinal vessels through the normal movement of blood in the capillaries, [9]. Compared with fluorescein angiography (FA), (OCTA) advantages are that it is non-invasive, acquires volumetric scans that can be segmented to specific depths, uses motion contrast instead of intravenous dye, can be obtained within seconds, provides accurate size and localization information, visualizes both the retinal and choroidal vasculature. As a disadvantage, (OCTA) has a limited field of view. So, we can distinguish:

- OCTA Small Field, which is limited to the posterior pole (macula and optic disc)
- OCTA Wide Field which allows analyzing a larger retinal area.

(OCTA) wide field can give more details on chorio-retinal vessels at the three different levels:

- Superficial capillary plexus (SCP): Layer of ganglion cells and nerve fibers
- Deep capillary plexus (DCP): Inner nuclear and outer plexiform layer
- Choriocapillary plexus (CC): Between the Bruch membrane (BM) and the Sattler layer, at the choroidal level.

Therefore, (OCTA) wide field is an imaging modality useful for the evaluation on RP disease, which mainly affects the periphery of the eyes.

In [10], we considered the images from OCTA Wide field of superficial capillary plexus, deep capillary plexus and choriocapillaris plexus of healthy subjects and retinitis pigmentosa (RP) patients.

 doi:10.20944/preprints202402.0883.v1

The images were referred to an experiment of 12 patients with previous diagnosis of either mid- or late-stage RP and a control group of 20 healthy age-matched subjects, at the University "G. d'Annunzio" of Chieti-Pescara, Italy.

We noticed that the main feature of images is that they present different levels of gray color therefore, by setting a threshold parameter for the gray level, we have a binary image with its own DF. Consequently, we obtain a variety of binary images depending on the threshold parameter, which reconstruct a curve of FDs depending on that parameter.

We have shown that, even when considering the possible variations indicated by the error bars, for most values of the parameter, the FD curve of images of healthy eyes is above that of images of patients with RP. For very small or very large values of the threshold parameter, we have a very distorted image, and the two curves seem almost coincident.

Another extension of OCT is **Spectral Domain Optical Coherence Tomography (SDOCT)** which provides high-resolution, optical cross-sectional, and en-face analysis of the retina and choroid with depth-resolved segmentation, [11]. SDOCT guarantees excellent focus with high-resolution visualization of the retina. There is a progressive decrease of signal towards the choroidal structures resulting in a decrease in the sensitivity and the resolution of images moving away from the zero-delay point (which corresponds to the inner retinal edge). There is a limitation of the dynamic range offered by the analog to digital conversion before the transformation of Fourier and the wavelength-dependent light scattering induces a reduction of the signal-noise contribution in the information coming from the lower retinal layers. An accurate study of the choroid is possible by performing SDOCT with Enhanced Depth Imaging (EDI) technology where the scan is closer to the eye of the patient to obtain an inverted image showing the deeper retinal layers and the choroid closer to the zero-delay point. This permits an enhanced and high-resolution image of the choroid up to the inner portions of the sclera [12,13]. Therefore, information on retinal architecture can be integrated with that on choroidal vasculature to better understand the pathogenesis of RP [14].

Choroid assessment in patients with RP has been the subject of study for several years, [15,16]. The role of the choroid in the pathogenetic mechanism of retinal damage in RP is not clear but it is now accepted that choroidal alterations participate as «primum movens» of damage. Impairment of the choroidal circulation leads to a reduction of the intraretinal vascular flow and, invariably, to retinal photoreceptor damage. The reduction of choroidal vascularization and reduction of retinal flow are probably associated with high values of plasma endothelin-1 (ET) in patients with RP.

In the present study, we will use spectral domain optical coherence tomography (SDOCT) to obtain choroidal images. The following SDOCT choroidal images refer to healthy eyes (right eye (a), left eye (b)) and were kindly provided by the group of Prof. S. Abdolrahimzadeh in "Sant'Andrea" Hospital of Rome (IT).

In the first part of the paper, we present the mathematical background, recall briefly fractals and fractal dimensions, multifractals and generalized Renyi point centered dimensions and then we present the algorithms we will use to calculate such dimensions.

In the second part, we present an experiment with two healthy subjects (Control Group) and three RP patients, which was done by the group of Prof. S. Abdolrahimzadeh at "Sant'Andrea" Hospital of Rome (IT). We analyze the choroid's vessels using SDOCT technique. We deduce at first the FD of the choroidal imaging for each pair of eyes, finding that it decreases in RP patients with respect to healthy subjects. Besides, due to choroidal vascular network being more properly a multifractal pattern, we calculate generalized Renyi point centered dimensions, finding that they are lower for the control group and increase in the patients with RP. At the end, there will be a discussion of the results obtained and conclusions will be drawn.

2. Mathematical background

2.1. Fractal Dimension

In this paragraph, we briefly revisit the concept of fractal dimension, and for a more in-depth exploration of fractals and fractal dimension, please refer to [17–21]. Let's consider an "object" existing

 doi:10.20944/preprints202402.0883.v1

in d dimensions. If $d = 1$, this "object" may consist of a set of line segments; for $d = 2$, it could be an assembly of parts from a plane; for $d = 3$, it might represent a section of three-dimensional space, and so on. It is widely acknowledged that we can attribute a "measure" M to this "object". In the case of $d = 1$, the "measure" corresponds to the length of the line segments; for $d = 2$, it represents the area of the plane parts; for $d = 3$, it signifies the volume of the three-dimensional part, and so forth.

To encompass this object, we can use "boxes" with a sufficiently small side length denoted as l. In the context of $d = 1$, these "boxes" are small line segments; for $d = 2$, they take the form of small squares; and for $d = 3$, they manifest as small cubes. If $\mathcal{N}(l)$ represents the minimum number of boxes with a side length of l required to cover the object, it becomes evident that,

$$M \approx \mathcal{N}(l)l^d$$

given that l^d serves as the length, area, or volume of each box. Solving the equation above in relation to d results in:

$$d \approx \frac{logM}{logl} + \frac{log\mathcal{N}(l)}{\log(l^{-1})}$$

As l is a negligible value and M is a constant, the term $logM/logl$ can be omitted. Hence,

$$d \approx \frac{log\mathcal{N}(l)}{log(l^{-1})}$$

The calculated value of d from the formula above may not be an integer. To be more accurate, the number D

$$D = \lim_{l\to 0} \frac{log\mathcal{N}(l)}{\log(l^{-1})} \tag{1}$$

can be any real number (less than the embedding dimension) and is termed the "Fractal Dimension" of the object mentioned above [18–21].

2.2. Multifractals

Let us examine a probability space denoted as $(\mathcal{X}, \mathcal{B}(\mathcal{X}), \mu)$. Assume $\mathcal{X} \subset \mathbb{R}^d$, and $\mathcal{B}(\mathcal{X})$ represents the Borel subsets of $\mathcal{X}$. Our focus is on situations where the probability measure μ on $\mathcal{B}(\mathcal{X})$ displays a high degree of irregularity, and the distribution is non-differentiable, with singularities of possibly many different orders. Such a measure is termed *multifractal*, [22].

Consider a lattice that encompasses the support of μ using d-dimensional boxes of side l. The box that contains x is denoted by $B_l(x)$, where $x \in \mathcal{X}_l$ and $\mathcal{X}_l = \{x: \mu[B_l(x)] > 0\}$. We evaluate successive lattice coverings for $l \longrightarrow 0$.

Let

$$K_l(y, \varepsilon) = \left\{x: y - \varepsilon < \frac{\log \mu[B_l(x)]}{\log l} \leq y + \varepsilon\right\} \tag{2}$$

The multifractal Spectrum denoted by $\tilde{f}(y)$ is defined to be

$$\tilde{f}(y) = \lim_{\varepsilon\to 0} \lim_{l\to 0} \frac{\log \#K_l(y, \varepsilon)}{\log(l^{-1})}$$

for $y > 0$. It is clear that this relation corresponds to (1) above. We will consider the Legendre transformation of $\tilde{f}(y)$

$$\tilde{\theta}(q) = \underbrace{inf}_{y} \{qy - \tilde{f}(y)\}$$

or equivalently

$$\tilde{\theta}(q) = qy - \tilde{f}(y) \text{ and } \frac{\partial\tilde{\theta}}{\partial q} = y, \frac{\partial\tilde{f}}{\partial y} = q$$

 doi:10.20944/preprints202402.0883.v1

From the last one, it is clear that if $\tilde{\theta}$ and $\tilde{f}$ depend on some parameter λ connected to healthy of not subjects, we have

$$\frac{\partial^2\tilde{\theta}}{\partial\lambda^2} = -\frac{\partial^2\tilde{f}}{\partial\lambda^2}$$

Hence for maximal values of $\tilde{f}(y)$ we will have minimal values of $\tilde{\theta}(q)$ and vice versa.
It can be proved that

$$\tilde{\theta}(q) = \lim_{l\to 0}\frac{\log\sum_{x\in X_l}\mu^q\big(B_l(x)\big)}{\log l} = \lim_{l\to 0}\frac{\log E(\mu^{q-1}\big(B_l(X)\big)}{\log l}$$

Instead of this, for the calculations, we consider the *point centered correlation exponents* defined as

$$\theta(q) = \lim_{l\to 0}\frac{\log\left(\int_{X_l}\mu^{q-1}\big(S_l(x)\big)\mu(dx)\right)}{\log l}$$

where $S_l(x)$ is a sphere of radius l centered at x. Then the *Generalized Renyi Point Centered Dimensions* are defined as

$$D_q = \begin{cases} \dfrac{\theta(q)}{q-1} & if \quad q \neq 1 \\ \lim\limits_{l\to 0}\dfrac{\int_{X_l}\log(\mu(S_l(x)))\,\mu(dx)}{\log l} & if \quad q = 1 \end{cases}$$

Theorem 1: Consider $X_1, X_2, \dots, X_q$ as a sample of independent random variables selected from the probability distribution μ. Define Y as follows

$$Y = max\{\|X_1 - X_q\|, \|X_2 - X_q\|, \dots, \|X_{q-1} - X_q\|\}$$

where $\|\cdot\|$ is the max norm. Then for $q = 2,3,4, \dots$

$$\int \mu^{q-1}\left(S_y(x)\right)\mu(dx) = Pr\{Y \le y\} \equiv F_Y(y)$$

Proof [22]:
Let **1**(A) be one if A is true and zero otherwise, then it is obvious that

$$\mu\big[S_y(x)\big] = \int \mathbf{1}\,(\|x_1 - x\| \le y)\mu(dx_1) = Pr\{\|X_1 - x\| \le y\}$$

Further,

$$\mu^{q-1}\big[S_y(x)\big] = \left[\int \mathbf{1}\,(\|x_1 - x\| \le y)\mu(dx_1)\right]^{q-1}$$

$$= \int \dots \int \mathbf{1}\,(\|x_1 - x\| \le y)\cdots\mathbf{1}\big(\|x_{q-1} - x\| \le y\big)\mu(dx_1)\cdots\mu\big(dx_{q-1}\big)$$

$$= \int \dots \int \mathbf{1}(\max\{\|x_1 - x\|, \dots, \|x_{q-1} - x\|\} \le y)\mu(dx_1)\cdots\mu\big(dx_{q-1}\big)$$

so,

$$\int \mu^{q-1}\big[S_y(x)\big]\,\mu(dx) =$$

$$= \int\int \dots \int \mathbf{1}(\max\{\|x_1 - x_q\|, \dots, \|x_{q-1} - x_q\|\}$$

$$\le y)\mu(dx_1)\cdots\mu\big(dx_{q-1}\big)\mu\big(dx_q\big)$$

$$= Pr\{Y \le y\}$$

Especially for q=2 we have

 doi:10.20944/preprints202402.0883.v1

$$Pr\{\|X_1 - X_2\| \le l\} = \int \mu(S_l(x))\mu(dx)$$

which is more or less expected.

From the above relations we have, for $q = 2,3,4, \ldots,$

$$\theta(q) = \lim_{y\to 0} \frac{\log F_Y(y)}{\log y}$$

Theorem 2: The correlation dimension exists iff the correlation integral $F_Y(y)$ can be decomposed in the following form

$$F_Y(y) = \Phi(y) y^{\zeta_q}$$

where ζ_q is a positive constant and $\Phi(y)$ is a positive function such that

$$\lim_{y\to 0} \frac{\log \Phi(y)}{\log y} = 0$$

Further, given this decomposition, $\theta(q) = \zeta_q$.

3. The algorithms

3.1. Computing the fractal dimension

To compute the fractal dimension of the images, we analyzed them first using mathematica, in order to extract the tree-shaped structure of the blood vessels. We checked each pixel of the image and if it belonged to a blood vessel (it had been black), we passed to the next pixel(s) of the particular blood vessel, by examining the neighboring pixels, reconstructing that way the blood vessel. Then we proceeded with fractal dimensional box-counting analysis as in [19] which is performed using Fractalyse (ThéMA, Besançon Cedex, France).

3.2. Computing the Generalized Renyi Point Centered Dimensions

3.2.1. The case when q = 2

Grassberger & Procaccia investigated the scenario with q = 2. Given a finite sequence of vector random variables $X_1, X_2, \ldots, X_N$ in $\mathbb{R}^d$, their approach involves computing all conceivable interpoint distances, and using these to construct an empirical distribution function as an estimate of $F_Y(y)$. That is, for q = 2,

$$\hat{F}_Y^{GP}(y, N) = \frac{2}{N(N-1)} \sum_{i=1}^{N-1} \sum_{j=i+1}^{N} \mathbf{1}\left(\|X_i - X_j\| \le y\right)$$

where **1**(A) is one if A is true and zero otherwise. The procedure then involves plotting $logy$ by sample values of $log\, \hat{F}_Y^{GP}(y, N)$, and using the slope of the line in some suitable region as an estimate of the correlation dimension $D_2 = \theta(2)$.

Our final step deviated slightly. We have found the $\hat{F}_Y^{GP}(y, N)$ as above for discrete values of y and fitted to the data the expression ay^b using mathematica. Then according to theorem 2 above $\theta(q) = b$.

3.2.2. The case when q = 2,3, ...

Given a finite sequence of vector random variables $X_1, X_2, \ldots, X_N$ in $\mathbb{R}^d$, define the random function $\hat{F}_Y^{GP}(y, N)$ as

$$\hat{F}_Y^{GP}(y, N) = \frac{1}{m} \sum_{k=1}^{m} \mathbf{1}(Y_k \le y)$$

 doi:10.20944/preprints202402.0883.v1

where $Y_1, Y_2, \dots, Y_m$ are all possible permutations of the qth order difference given a sample of N points, the kth being

$$Y_k = max\left\{\left\|X_{k_1} - X_{k_q}\right\|, \left\|X_{k_2} - X_{k_q}\right\|, \dots, \left\|X_{k_{q-1}} - X_{k_q}\right\|\right\}$$

In cases where q > 2, one samples X_{k_q} from $X_1, X_2, \dots, X_N$ *without* replacement. Subsequently X_{k_i} for $i = 1,2, \dots, q-1$ is sampled *with* replacement. In this second phase, there are N^{q-1} possibilities, and in the first phase, there are N possibilities. Therefore $m = N(N-1)^{q-1}$. The function $\hat{F}_Y^{GP}(y, N)$ is an estimator of $F_Y(y)$.

We implemented the above algorithm as follows. We know that every image is a collection of pixels, actually a 2-dimensional array of pixels. Every pixel has a luminosity equal to some value. So, a picture corresponds to a matrix with elements of pixel's luminosities. We normalized these values and interpolated between them, so we had a 2-dimensional Probability Density Function, i.e. a probability distribution μ. Then we gave values to $X_1, X_2, \dots, X_N$ for $N = 100$ according to the distribution μ and computed as above the $\hat{F}_Y^{GP}(y, N)$ for 10 values of y which is an estimation of $F_Y(y)$.

Finally, we fitted to the points of $\hat{F}_Y^{GP}(y, N)$ the expression ay^b for a, b constants using mathematica. Then according to the above theorem 2 $\theta(q) = b$.

4. Results

In the present paper, we consider two healthy subjects (Control Group) which correspond to images 1, 2, 3a, 3b and three patients:

- A patient with homozygous PDE6b mutation which corresponds to images of Figure 1 A, B of [23]
- A myopic patient with rhodopsin rhoAsp190Asn mutation which corresponds to Figure 2 A, B of [23]
- A patient with Usher's disease, a genetic syndromic illness associated with RP also involves ear and balance problems which corresponds to Figure 3 A, B of [23].

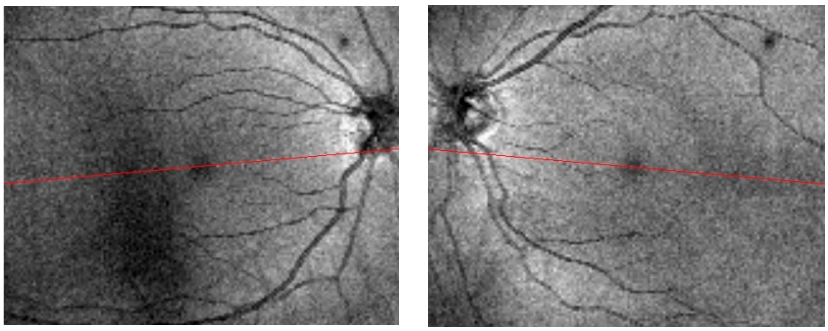

Healthy Right Eye (a) Healthy Left Eye (b)

Figure 1. SDOCT choroidal images referring to healthy eyes (right eye (a), left eye (b)).

4.1. Fractal dimension

For the previous two healthy subjects and three patients, we deduced at first the FD of choroid's vessels.

We get the results of the Tables below, where r^2 is a measure of the quality of the linear regression analysis in our model ($r^2 = 1$ means best fitting). Fractalyse uses the p – value approach to hypothesis testing. Since p - values are very small, there is strong evidence that $log\mathcal{N}(l)$, $\log(l^{-1})$ are linearly related.

 doi:10.20944/preprints202402.0883.v1

Table for Right Eye

Image	FD	r^2	Confidence (95%)	p-value
1 CG	1.557	0.999	1.510-1.604	2.308E-10
3a CG	1.485	1.000	1.456-1.514	1.838E-11
Figure 1A	1.167	0.997	1.096-1.237	1.350E-07
Figure 2A	1.130	0.999	1.083-1.177	2.092E-08
Figure 3A	0.907	0.992	0.815-0.998	1.758E-06

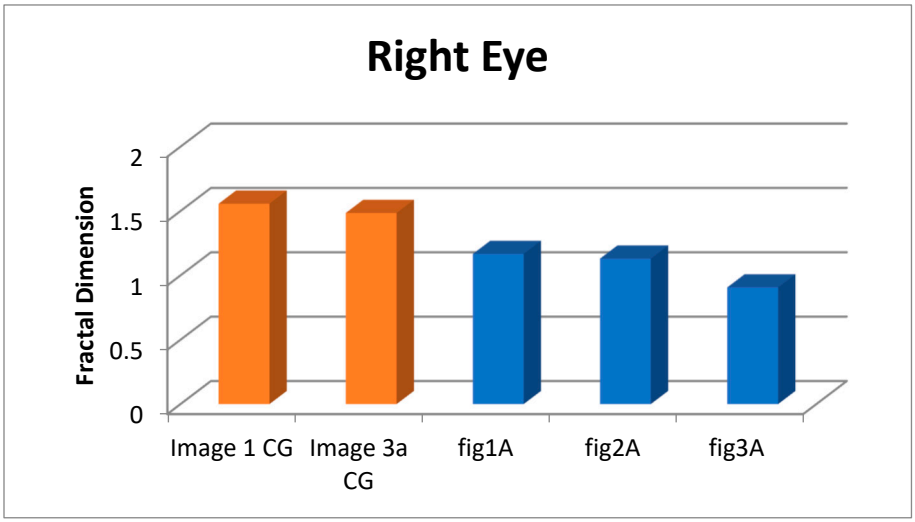

Table for Left Eye

Image	FD	r^2	Confidence (95%)	p-value
2 CG	1.307	0.989	1.172-1.443	3.803E-07
3b CG	1.071	0.999	1.034-1.108	5.337E-10
Figure 1B	1.055	0.996	0.981-1.128	2.733E-07
Figure 2B	0.981	0.999	0.944-1.018	1.328E-08
Figure 3B	1.087	0.990	0.964-1.211	3.172E-06

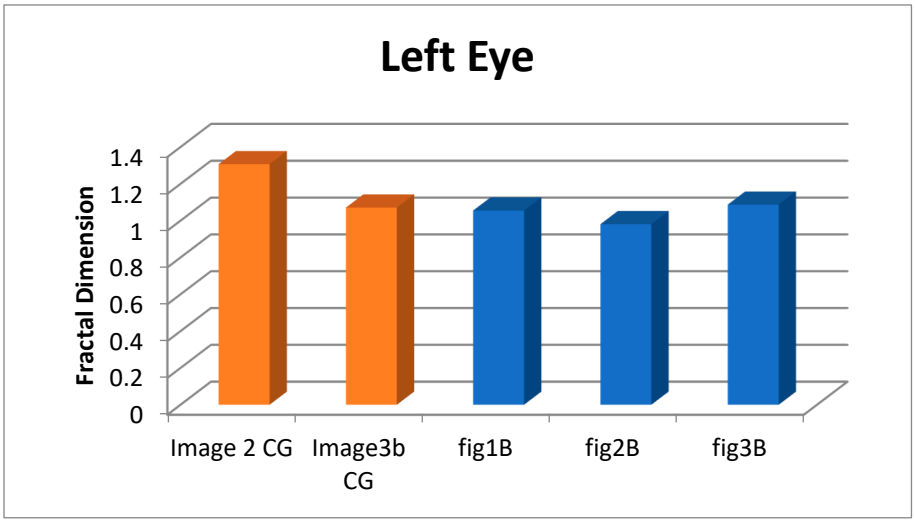

 doi:10.20944/preprints202402.0883.v1

We can observe that, even if the literature refers RP as a bilateral pathology, it seems that the right eye is mostly affected. Besides, among the three pathologies, the Usher's disease seems to be the most serious.

4.2. Generalized Renyi point centered dimensions

A multifractal set can be seen as the union of several mono-fractal subsets, among them *freely interconnected*, each having its own dimension fractal.

Such a union can be described **entirely by an infinite number of generalized dimensions D**, also called Renyi's i.e. across the **spectrum f**, known as the multifractal spectrum.

Another important index, used in literature for multifractal analysis, is the generalized Renyi point centered dimensions, which represent a measure of inhomogeneity of data, [22].

The chorioretinal vascular network could be more properly considered a multifractal pattern because its different regions have different fractal properties characterized by an infinite number of generalized dimensions, rather than a single fractal dimension.

Therefore, we calculated the generalized Renyi point centered dimensions for our case study. We obtained the results which are summarized in the following graphs:

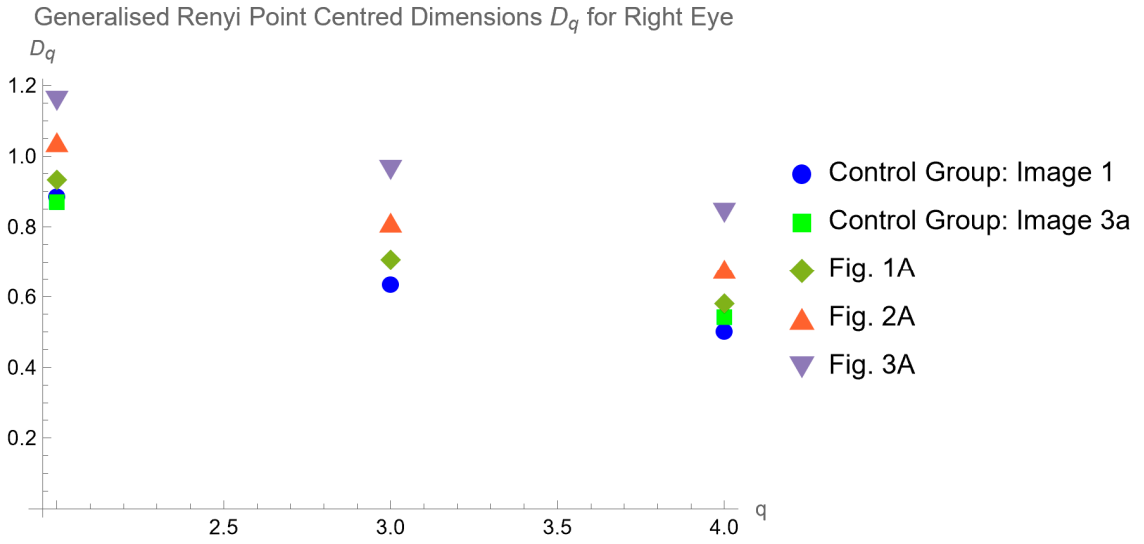

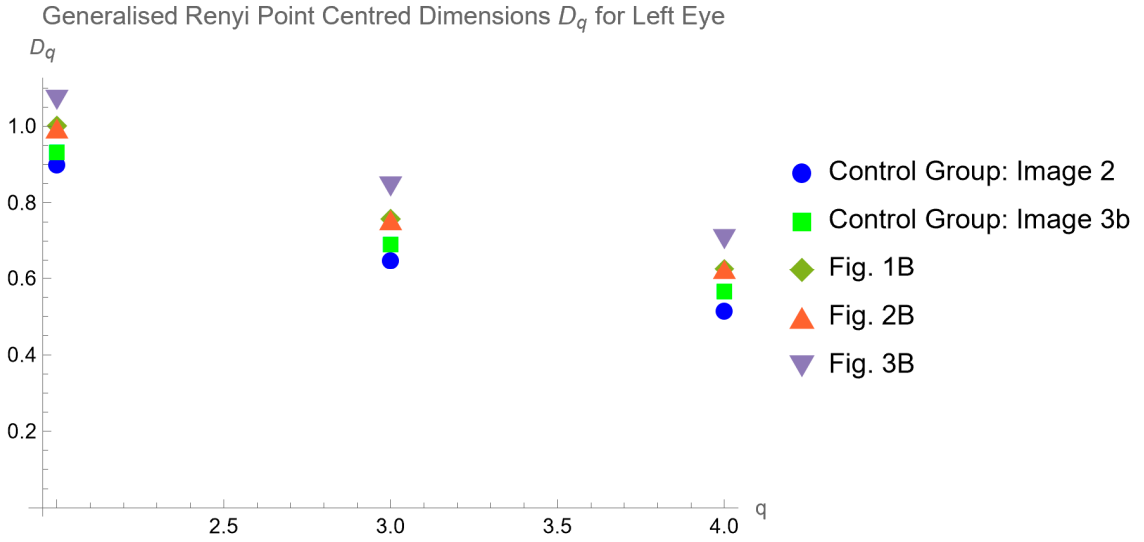

5. Discussion

In the present experiment, we analyzed a case study of two healthy subjects and three RP patients. We studied the choroid's vessels using SDOCT technique. We deduced at first the FD of the

 doi:10.20944/preprints202402.0883.v1

choroidal imaging for each pair of eyes, finding that it decreases in RP patients with respect to healthy subjects. This means that, in the genetic pathology of retinitis pigmentosa, the tree of choroidal vascularization has fewer branching connections, therefore the geometry of the choroid becomes more simplified. Consequently, a complete and efficient vision is not allowed to the patients from a young age, and the visual ability degenerates further with aging.

Besides, due to the choroidal vascular network being more properly a multifractal pattern, we calculated generalized Renyi point centered dimensions, finding that they are lower for the control group and increase in the patients with RP, mostly in the Usher's case. This is compatible with the mathematical dependence between FD and generalized Renyi point centered dimensions.

6. Conclusions

New imaging techniques together with computer science and multifractal analysis can be very useful in RP disease for early diagnosis, which represents the only defense against this rare genetic illness. According to the clinical observation that choroid's alterations of vascular circulation lead to photoreceptors damage, we focused on choroidal images, using the new technique of spectral domain optical coherence tomography (SDOCT).

Due to the multifractal structure of the choroid's blood vessels, we used the generalized Renyi point centered dimensions, as a measure of inhomogeneity of data. We showed, in a study case, that generalized Renyi point centered dimensions of the choroidal images increase in the patients with RP with respect to those of healthy subjects. It could be due to the rise of inhomogeneity in the images. This result enables us to propose the generalized Renyi point centered dimensions as an index to warn of the presence of RP pathology.

As a future work, we aim to perform the study on a number of patients that allow a quantitative comparative estimation and a complete statistical analysis. It would be important to set a percentage of comparison with other non-genetical chorio-retinal pathologies such as diabetic retinopathy or glaucoma. In general, we can suppose from our research that generalized Renyi point centered dimensions of the choroidal images in RP, in mature age, are uper as compared with those of non-genetical illness.

Anyway, before moving on to clinical applications, it is necessary that a standardized protocol for image acquisition/processing be established first to facilitate inter-study comparison.

Author Contributions "Conceptualization and methodology", De Sanctis, A. A." Software and formal analysis", Oikonomou, F. D." Medical investigation and data curation", Minicucci, F. All authors have read and agreed to the published version of the manuscript.

Funding: This research received no external funding.

Institutional Review Board Statement: The study is purely scientific and does not involve any type of clinical experimentation on human subjects, anyway it was conducted in accordance with the Declaration of Helsinki.

Informed Consent Statement: Informed consent was obtained from all subjects involved in the study.

Data Availability Statement: The (SDOCT) images were kindly provided by the group of Prof. S. Abdolrahimzadeh in "Sant'Andrea" Hospital of Rome (IT).

Conflicts of Interest: The authors declare no conflict of interest.

References

1. Verbakel, S.K.; Van Huet, R.; Boon, C.; den Hollander, A.I.; Collin, R.; Klaver, C. et al. Nonsyndromic retinitis pigmentosa. *Prog. Retin. Eye Res.* 2018, 66, 157–86.
2. Marigo, V. Programmed cell death in retinal degeneration: targeting apoptosis in photoreceptors as potential therapy for retinal degeneration. *Cell Cycle,* 2007, 6, 652–5.
3. Ferrari, S.; Di Iorio, E.; Barbaro, V.; Ponzin, D.; Sorrentino, F.S.; Parmeggiani, F. Retinitis pigmentosa: genes and disease mechanisms. *Curr. Genomics*. 2011, 12, 238–49.

4. Campbell, J.P.; Zhang, M.; Hwang, T.S.; Bailey, S.T.; Wilson, D.J.; Jia, Y.; Huang, D. Detailed Vascular Anatomy of the Human Retina by Projection-Resolved Optical Coherence Tomography Angiography. *Sci. Rep.* 2017, 7, 42201. doi:10.1038/srep42201.
5. Family, F.; Masters, B.R.; Platt, D.E. Fractal Pattern Formation in Human Retinal Vessels. *Phys. Nonlinear Phenom*. 1989, 38, 98–103; doi:10.1016/0167-89(89)90178-4.
6. Lakshminarayanan, V.; Raghuram, A.; Myerson, J.; Varadharajan, S. The Fractal Dimension in Retinal Pathology. *J. Mod. Opt. - J MOD Opt*. 2003, 50, 1701–1703; doi:10.1080/0950034031000069442.
7. Yu, S.; Lakshminarayanan, V. Fractal Dimension and Retinal Pathology: A Metaanalysis, Appl. Sci. 2021, 11, 2376. Available online: https://doi.org/10.3390/app11052376 (accessed on 9.9.2021).
8. Mitamura, Y.; Mitamura-Aizawa, S.; Nagasawa, T.; Katome, T.; Eguchi, H.; Naito,T. Diagnostic imaging in patients with retinitis pigmentosa. *J. Med. Invest.* 2012, 59, 1–11.
9. Jauregui, R.; Park, K.S.; Duong, J.K.; Mahajan, V.B.; Tsang, S.H. Quantitative progression of retinitis pigmentosa by optical coherence tomography angiography. *Sci. Rep*. 2018, 8, 13130.
10. Minicucci F.; Oikonomou F. D. and De Sanctis A. A. Fractal dimensional analysis for retinal vascularization images in retinitis pigmentosa: a pilot study. *Chaos, Fractals and Complexity*, Springer Proceedings in Complexity, 2023.
11. Spaide R.F.; Koizumi H.; Pozzoni M.C. Enhanced depth imaging spectral-domain optical coherence tomography. *Am J Ophthalmol*. 2008, 146, 496–500.
12. Margolis R.; Spaide R.F. A pilot study of enhanced depth imaging optical coherence tomography of the choroid in normal eyes. *Am J Ophthalmol*. 2009, 147, 811–5.
13. Chhablani J.; Wong I.Y.; Kozak I. Choroidal imaging: a review. *Saudi J Ophthalmol*.2014, 28, 123–128.
14. Zhang Y.; Harrison J. M.; Nateras O. S.; Chalfin S.; Duong T. Q. Decreased retinal-choroidal blood flow in retinitis pigmentosa as measured by MRI. *Doc Ophthalmol*. 2013, 126, 187–97.
15. Finzi A.; Cellini M.; Strobbe E.; Campos EC. ET-1 plasma levels, choroidal thickness and multifocal electroretinogram in retinitis pigmentosa. *Life Sci*. 2014, 118, 386–90.
16. Strobbe E.; Cellini M.; Fresina M.; Campos EC. ET-1 plasma levels, aqueous flare, and choroidal thickness in patients with retinitis pigmentosa. *J Ophthalmol*. 2015, 292615.
17. Mandelbrot, B.B.; Wheeler, J.A. The Fractal Geometry of Nature. *Am. J. Phys.* 1983, 51, 286–287; doi: 10.1119/1.13295.
18. Mandelbrot, B.B. *Les Objets Fractals*; Flammarion: Paris, France, 1999.
19. Falconer, K. *Fractal Geometry Mathematical Foundations and Applications*, John Wiley & Sons: England, 1990.
20. Barnsley, M.F. *Fractals Everywhere*, 3d ed.; Academic Press: San Diego, USA, 1993.
21. Peitgen, Heinz-Otto; Jürgens, H.; Saupe, D. *Chaos and Fractals*, Springer: New York, USA, 2004.
22. Harte, D. *Multifractals theory and applications*; CHAPMAN & HALL/CRC Boca Raton, London, New York, Washington, D.C. © 2001.
23. Abdolrahimzadeh S.; Di Pippo M.; Ciancimino C.; Di Staso F. and Lotery A. J. Choroidal vascularity index and choroidal thickness: potential biomarkers in retinitis pigmentosa. *Eye*, Springer Nature, 2022.